Journal for ImmunoTherapy of Cancer

Novel combination strategy of high intensity focused ultrasound (HIFU) and checkpoint blockade boosted by bioinspired and oxygen-supplied nanoprobe for multimodal imaging-guided cancer therapy

Rui Tang,[1,2] Hongye He,[1,2] Xiaohong Lin,[2,3] Nianhong Wu,[1,2] Li Wan,[1,2] Qiaoqi Chen,[1,2] Yaqin Hu,[1,2] Chen Cheng,[1,2] Yuting Cao,[1,2] Xun Guo,[1,2] Ying Zhou,[1,2] Xialin Xiong,[1,2] Min Zheng,[1,2] Qi Wang,[4] Faqi Li,[4] Yang Zhou,[5] Pan Li [1,2]

To cite: Tang R, He H, Lin X, *et al*. Novel combination strategy of high intensity focused ultrasound (HIFU) and checkpoint blockade boosted by bioinspired and oxygen-supplied nanoprobe for multimodal imaging-guided cancer therapy. *Journal for ImmunoTherapy of Cancer* 2023;**11**:e006226. doi:10.1136/jitc-2022-006226

► Additional supplemental material is published online only. To view, please visit the journal online (http://dx.doi.org/10.1136/jitc-2022-006226).

RT, HH and XL contributed equally.

Accepted 22 December 2022

For numbered affiliations see end of article.

Correspondence to
Dr Pan Li;
lipan@hospital.cqmu.edu.cn

ABSTRACT

Background High-intensity focused ultrasound (HIFU) has shown considerable promise in treating solid tumors, but its ultrasonic energy is easily attenuated, resulting in insufficient energy accumulation in the target area. Moreover, HIFU ablation alone may inevitably lead to the presence of residual tumors, which may cause tumor recurrence and metastasis. Here, we describe a synergistic regimen combining HIFU facilitation with immunomodulation based on a novel oxygen-carrying biomimetic perfluorocarbon nanoparticle (M@P-SOP) to stimulate immunogenic cell death in tumor cells while alleviating immune suppression tumor microenvironment.

Methods M@P-SOP was prepared by double emulsion and film extrusion method. The anticancer and antimetastatic effects of M@P-SOP were evaluated on a preclinical transplanted 4T1 tumor model by combining HIFU and immunotherapy. Flow cytometry and immunofluorescence were used to clarify the potential mechanism of HIFU+M@P-SOP and their role in anti-programmed death ligand-1 (PD-L1) therapy.

Results Guided by photoacoustic/MR/ultrasound (US) multimodal imaging, M@P-SOP was abundantly enriched in tumor, which greatly enhanced HIFU's killing of tumor tissue in situ, induced stronger tumor immunogenic cell death, stimulated dendritic cell maturation and activated $CD8^+$ T cells. At the same time, M@P-SOP released oxygen to alleviate the tumor hypoxic environment, repolarizing the protumor M2-type macrophages into antitumor M1-type. With concurrent anti-PD-L1 treatment, the antitumor immune response was further amplified to the whole body, and the growth of mimic distant tumor was effectively suppressed.

Conclusions Our findings offer a highly promising HIFU synergist for effectively ameliorating acoustic and hypoxia environment, eventually inhibiting tumor growth and metastasis by stimulating host's antitumor immunity under HIFU ablation, especially in synergizing with PD-L1 antibody immunotherapy.

WHAT IS ALREADY KNOWN ON THIS TOPIC

⇒ High-intensity focused ultrasound (HIFU) has demonstrated promise for the treatment of solid tumors in clinical settings, however, its therapeutic efficiency is limited as the ultrasonic energy is easily attenuated and HIFU ablation alone may inevitably face the challenge of residual tumors.

WHAT THIS STUDY ADDS

⇒ Here, a combined therapeutic modality of nanoparticle-augmented HIFU ablation and anti-PD-L1 immunotherapy has been developed for high-efficient synergistic cancer treatment based on elaborately designed M@P-SOP nanocapsules. The immunogenic cell death of cancer cells by HIFU, immunosuppressive hypoxic tumor microenvironment attenuation by directly O_2 releasing from M@P-SOP and T-cell response enhancement by PD-L1 blockade collectively activated systemic immune response, consequently suppress local and distant tumor growth, which can be guided by ultrasound, MR and photoacoustic trimodality imaging.

HOW THIS STUDY MIGHT AFFECT RESEARCH, PRACTICE OR POLICY

⇒ This study develops an enhanced combination therapy with HIFU and immunotherapy, to inhibit tumor growth and metastasis based on the nano-biotechnology (nanoparticles as the synergistic agent and oxygen carrier), offering a new and efficient therapeutic protocol for clinic cancer treatment.

BACKGROUND

High-intensity focused ultrasound (HIFU) is generally considered to be one of the most representative non-invasive therapeutic strategies for thermal ablation and

mechanical destruction of tumor tissues using focused ultrasound (US) waves.[1] This modality has shown considerable promise in treating solid tumors, including breast, pancreas, liver, kidney, and prostate cancer.[2 3] However, the US radiation energy decays exponentially with increasing tissue depths and blood perfusion rates, which leads to insufficient energy accumulation in focal region, thus compromising the therapeutic efficiency of HIFU.[4] Classical strategy to strengthen ablation efficacy of HIFU is to increase the acoustic power or prolong the operation duration, but these options may lead to adverse biological effects such as transient pain, skin or nerve injury.[5 6] Some investigations have confirmed that the introduction of synergistic agents (SAs) is an efficient and alternative route to enhance HIFU surgical efficacy.[7 8]

Microbubbles (MBs), as one of the most commonly used SAs, can effectively improve the acoustic environment (AET) and intensify the US energy deposition via enhanced thermal and cavitation effects.[3 9] However, their micron-level size prevents them from permeating tumor tissues. Meanwhile, due to the poor stability, short half-life and uncontrollable cavitation scope, the clinical application of MBs is hindered.[10] Recently, various liquid-gas phase-changeable perfluorocarbon (PFC) nanoparticles (NPs) have been constructed as HIFU SAs,[5 11] which exhibit remarkable superiorities and potentials compared with MBs, such as extended circulation time, higher stability and easy modification.[12] Theoretically, based on the nanometer scale of NPs, they can pass through microvascular endothelial barrier into tumor tissue, which can further be in situ turned into MBs by HIFU triggering,[9 11] thus improving the ablation efficiency. It is noted that we have successfully synthesized temperature-responsive phase-transformation NPs in previous works for precise ultrasonography and enhanced HIFU surgery.[13 14]

Nonetheless, on the other hand, HIFU ablation alone may inevitably lead to the persistence of residual tumors, which can further result in tumor recurrence and metastasis.[15] Fortunately, accumulating evidences have demonstrated that many local cancer therapies such as HIFU can also cause tumor-associated antigens release, subsequently activating specific antitumor immune responses,[2 16–19] which provides a rationale to combine this ablative technique with systemic immunotherapy to produce synergistic effects. Researches on the combination of immunotherapy with HIFU have been carried out in some studies. For instance, preclinical evidence has revealed that combining HIFU with anti-cytotoxic T lymphocyte antigen-4 antibody (αCTLA-4) and anti-programmed death ligand 1 antibody (αPD-L1), two typical immune checkpoint inhibitors (ICIs), notably improves antitumor effect, increasing survival rate from 0% to 62.5% in a murine neuroblastoma model.[17] Pretreatment with an immune agonist (toll-like receptor 9 activator CpG) and modulation of programmed death 1 (PD-1)/PD-L1 axis before HIFU drives a highly effective systemic immune response and generate a durable cure in various cancer models.[20 21] However, vascular occlusion during HIFU may exacerbate tumor hypoxia,[22] which aggravates the immunosuppressive tumor microenvironment (TME) and compromises the synergistic therapeutic effect of HIFU and immunotherapy.

Hypoxic TME can stimulate the reeducation of macrophages to pro-tumoral M2-type, sabotage cytotoxic T lymphocytes (CTLs) mediated anticancer responses, increase the recruitment of regulatory T cells, as well as upregulate PD-L1 level on tumor and myeloid-derived suppressor cells.[23–25] Hence, rational strategies to regulate the hypoxic TME are crucial to reverse hypoxia-associated immunosuppression. Studies have shown that tumor hypoxia can be improved by carrying oxygen externally[26] or generating oxygen endogenously.[27 28] Intriguingly, PFC aforementioned such as perfluorohexane (PFH) is one of the most fascinating carriers for O_2 delivery owing to its excellent binding capacity with oxygen.[29] n addition, using HIFU to trigger oxygen release from PFC can enhance its low passive O_2 release efficiency.[26] Therefore, phase-changeable PFH NPs can not only serve as an idea SA for HIFU treatment but as an excellent O_2 vector to simultaneously mitigate hypoxia TME. So far, for all we know, the combination of HIFU, hypoxia alleviation and PD-L1 blockade immunotherapy has never been explored. Herein, we proposed that integrating immune checkpoint blockade with the anticancer effects induced by HIFU and hypoxia alleviation with the application of O_2-carried PFH NPs would evoke robust cooperative antitumor effects, providing a novel tactic for cancer therapy. However, the prerequisite to achieve the above goal is the efficient accumulation of NPs in tumor tissue before HIFU irradiation. Traditionally, to enhance the targeting ability of NPs, a wide range of targeting ligands can be modified on NPs, such as small molecules, aptamers, peptides, and antibodies; however, the non-specific scavenging and low biological compatibility remain challenging, and the preparation procedures are often complicated and laborious.[30] In this situation, biomimetic camouflaged nanotechnology, as a top-down approach, has received growing attention for enabling target-specific drug delivery while bypassing the tedious group-modified engineering.[31–33] In particular, cancer cell membrane (CCM) coated particles, with their inherited affinity ligands from the parent cells, can actively target homologous tumors.[34]

In the present work, a multifunctional hybrid nanoplatform (designated as M@P-SOP) has been developed to achieve HIFU facilitation and hypoxia improvement for cancer immunotherapy (figure 1). Owing to its low toxicity, biocompatibility and Food and Drug Administration approval, poly (lactic-co-glycolic acid) (PLGA) was selected to be a favored substance for drug delivery. The CCM coating on the surface would endow the NPs with homologous tumor targeting capabilities. The phase-changeable PFH, with low boiling point (56 ℃),[35] in the core could carry O_2 and be transformed into MBs by HIFU stimulation, synchronously improving the HIFU-ablation efficacy and mitigating hypoxic microenvironment. Subsequently, the HIFU induced-immunogenic cell

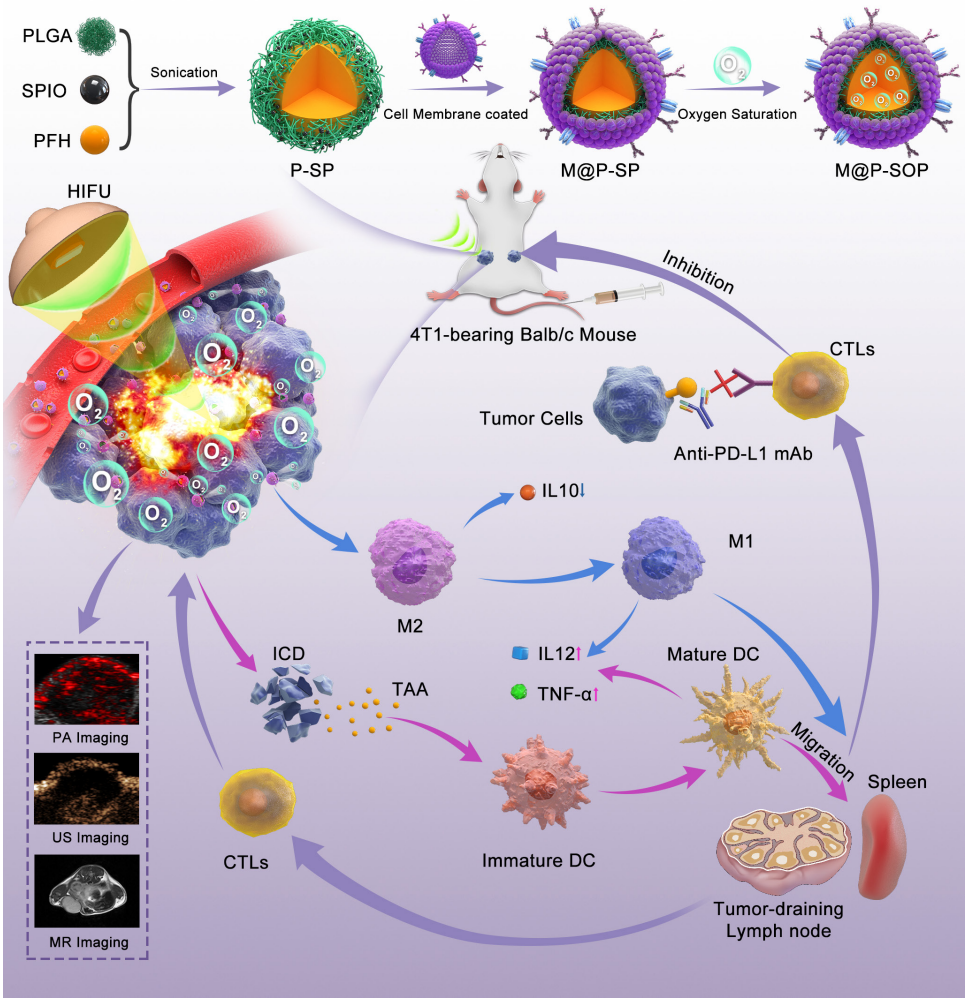

Figure 1 Schematic illustration of the preparation of M@P-SOP, the synergistic effects and mechanism of M@P-SOP-augmented HIFU in combination with anti-PD-L1 blockade against primary and distant tumors. DC, dendritic cell; HIFU, high-intensity focused ultrasound; ICD, immunogenic cell death; PA, photoacoustic; PFH, perfluorohexane; PLGA, poly (lactic-co-glycolic acid); SPIO, superparamagnetic iron oxide; TAA, tumor-associated antigen; US, ultrasound.

death (ICD) and hypoxia alleviation collectively promote the generation of immune-activating TME. By administrated with the checkpoint therapy (αPD-L1) to increase T-cell response, M@P-SOP-augmented HIFU irradiation exerted notable abscopal effects, suppressing the growth of distant tumor. Furthermore, M@P-SOP could also realize complementary multimodal-imaging including US imaging (USI) by PFH, T_2-weighted MRI and photoacoustic imaging (PAI) by superparamagnetic iron oxide (SPIO). In summary, the elaborately designed multifunctional NP shows a promising application in imaging-guided enhanced cancer treatment, and is capable of synergizing with HIFU and anti-PD-L1 blockade to jointly curb tumor growth and metastases.

METHODS

Materials

PLGA (molecular weight: 12 kDa) was acquired from Jinan Daigang Biotechnology (Jinan, China). SPIO was obtained from Ocean Nano (AR, USA). PFH was ordered from Elf Atochem (MA, USA). Tris (4,7-diphenyl-1,10-phenanthroline) ruthenium (II) dichloride ($[Ru(dpp)_3]Cl_2$) was supplied by Alfa Aesar (Shanghai, China). Hypoxyprobe Plus Kit was obtained from Hypoxyprobe (Burlington, Massachusetts, USA). ELISA kits were acquired from Elabscience Biotechnology (Wuhan, China). Anti-mouse PD-L1 (B7-H1) was provided by Bioxcell (USA). Antibodies for flow cytometry (FCM) analysis were obtained from BioLegend (California, USA).

Preparation and characterization of M@P-SOP

M@P-SOP was prepared based on the previous methods with some modifications.[36] First, 4T1 cell membranes were collected using a membrane protein extraction kit (Beyotime Biotechnology, Shanghai, China). PLGA encapsulating SPIO and PFH (P-SP) was fabricated via a typical double-emulsion method according to our previous report.[13] For targeted delivery, 4T1 CCM was modified on P-SP via a coextrusion method.[37] Briefly, P-SP and CCM were fully mixed and extruded 10–12 times through a 1 μm polycarbonate membrane. After fully

being saturated with oxygen for 2–3 hours (4°C), M@P–SOP was obtained. In order to further bestow M@P-SOP with fluorescence imaging capacity, classic fluorescence dye DiI or DiR was added during the synthesis procedure.

The structure was detected with transmission electron microscope (TEM, Hitachi H-7600, Japan). The morphology was observed under confocal microscope (CLSM, Carl Zeiss, Germany). The size and zeta potential were evaluated with dynamic laser scattering (Malvern Instruments, UK). The encapsulation efficiency (EE) of SPIO was detected with inductively coupled plasma optical emission spectrometer. The paramagnetic behavior was detected by a physical property measurement system. The protein expression pattern was identified by sodium dodecyl sulfate polyacrylamide gel electrophoresis. Phase change process was examined via a light microscope with a heating table. The oxygen releasing was tested using portable dissolved oxygen meter (JPBJ-608, Shanghai, China).

Cell culture and experimental animals

4T1, MCF-7, MDA-MB-231, and B16F10 were grown in RPMI-1640 medium with addition of 10% FBS and 1% penicillin-streptomycin under recommended condition (5% CO_2, 37 °C). Female Balb/c mice (6–8 weeks) were obtained from Ensiweier Biotechnology (Chongqing, China). Female Kunming mice (6–8 weeks) were supplied by the Laboratory Animal Center of Chongqing Medical University. The primary tumor-bearing model was set up by infection of 1×10^6 4T1 cells into the right mammary fat pad of Balb/c mouse (unilateral model). Four days later, an artificial bilateral model was created by infection of 5×10^5 4T1 cells into the left to mimic a distant metastatic tumor.

In vitro homologous targeting ability and in vivo biodistribution of M@P-SOP

4T1 cells (1×10^5/dish) seeded in CLSM dishes were treated with DiI-labeled P-SOP or M@P-SOP for 0.5, 1, 2 and 4 hours, respectively. After 20 min of incubation with 4',6-diamidino-2-phenylindole (DAPI), the cells were observed under CLSM and assayed via FCM (Cytoflex, USA). Additionally, 4T1, MCF-7, MDA-MB-231, and B16F10 were treated with DiI-labeled M@P-SOP for 4 hours, respectively. The uptake level of nanoprobes was detected with CLSM and FCM too.

Mice with unilateral 4T1 tumor were intravenously administrated with DiR-labeled P-SOP or M@P-SOP (5 mg/mL, 200 µL), respectively. Fluorescence imaging (Xenogen IVIS Spectrum, PerkinElmer, USA) was conducted 1, 3, 6, 24 and 48 hours after injection. Another six mice (n=3) were executed at 24 hours, with vital organs and tumors assessed by fluorescence imaging.

In vitro and in vivo USI/PAI/MRI

To determine the USI performance of M@P-SOP in vitro, a 3% agarose gel phantom with holes was constructed and added with HIFU-irradiated PBS (control), M@P-SOP, M@P-SP or M@P-S, respectively. The B-mode and contrast mode images were captured using MyLab90 ultrasonograph (Esaote, Italy). In addition, unilateral 4T1 tumor-bearing mice were intravenously administrated with P-SOP or M@P-SOP (5 mg/mL, 200 µL). After 24 hours, the same instrument was employed to collect B-mode and contrast mode images at tumor site before and after HIFU. DFY software (independently invented by the Institution of Ultrasound Imaging of Chongqing Medical University, China) was used for evaluation of the ultrasonic intensity values.

Similarly, PAI of M@P-SOP NPs was executed using Vevo LAZR PAI apparatus (Visual Sonics, Toronto, Canada) at 690 nm. MRI of M@P-SOP was conducted on an MRI instrument (Siemens Prisma, 3.0T, Germany) and analyzed via Syngo Via software. For in vivo PAI/MRI, the imaging was performed at pre, 1, 3, 6, 24 and 48 hours post P-SOP or M@P-SOP injection. MRI parameters: T_2WI: (repetition time/echo time: 8340/85 ms, FOV: 80×100 mm. T_2MAP: (repetition time/echo time: 2000/14.6 ms, FOV: 95×100 mm).

Ex vivo and in vivo HIFU synergistic ablation

Fresh bovine livers (150 mm×150 mm×100 mm) were degassed by vacuum pump for 60 min, then placed into HIFU system (JC-200, Chongqing Haifu Medical Technology, China). 200 µL of saline, M@P, M@P-S or M@P–SOP were injected into the livers. HIFU (90 W, 120 W and 150 W) was conducted immediately at the injection site for 3 s. The livers were taken out and sliced layer by layer along the acoustic beam until the maximum damage section was found and photographed.

Unilateral tumor-bearing mice were ntravenously administrated with 200 µL M@P-SOP, M@P-S, M@P or saline. 24 hours later, HIFU treatment (120 W, 3 s) against tumor was performed under US guidance. US images were collected before and after ablation. The gray scale values were calculated automatically. Then, the tumors were incubated with 2,3,5-Triphenyltetrazolium chloride (TTC) dye. The volume (V) of coagulated necrotic tissue was measured and energy efficiency factor (EEF) was analyzed. V (mm^3) = $\pi/6\times$length × width×thickness. EEF (J/mm^3) = $\eta PT/V$. η was the focusing coefficient (= 0.7). P (W) and T (s) were the acoustic power and time.

In vitro and in vivo hypoxia assays

4T1 cells (5×10^5/well) in 12-well plates were cultured in hypoxia condition for 12 hours, followed by treatment of PBS under normoxia (negative control), or PBS (positive control), 2.5 or 5 mg/mL M@P-SOP under hypoxia for another 12 hours. $[Ru(dpp)_3]Cl_2$ (an O_2 indicator, 10 mg/mL) was then added. After 12 hours, the plates were examined under an inverted fluorescence microscope.

4T1 tumor-bearing mice were randomized and i.v. administrated with 200 µL M@P-SP, M@P-SOP (5 mg/mL) or saline, with or without HIFU irradiation (120 W, 3 s) 24 hours postinjection. The Hypoxyprobe-1 Plus Kit was applied to evaluate tumor hypoxia level. Briefly,

mice were intraperitoneally administered with pimonidazole hydrochloride (60 mg/kg). After 1.5 hours, the tumors were excised, sliced and stained with anti-pimonidazole or anti-hypoxia inducible factor-1α (HIF-1α) antibodies. FCM was conducted to determine the M1 ($CD11b^+F4/80^+CD80^+$) and M2 ($CD11b^+F4/80^+CD206^+$) macrophages in tumors. Serum cytokines including tumor necrosis factor-α (TNF-α), interleukin-10 (IL-10), and interleukin-12 (IL-12) were examined using ELISA.

In vivo HIFU+M@P-SOP synergistic PD-L1 blockade

Bilateral tumor-bearing mice were randomly grouped as follows: Control, PD-L1, HIFU, HIFU+NPs, HIFU+PD-L1, HIFU+NPs+PD-L1. On day 0, the mice were intravenously administrated with 200 µL M@P-SOP (5 mg/mL) or saline. HIFU (120 W, 3 s) irradiation was conducted on primary tumor 24 hours later. Anti-PD-L1 antibodies (1.5 mg/kg) were administered i.v. on days 2, 5 and 8. Mice weights were measured every other 2 days for 15 days. The tumor weights were measured on day 15. The primary tumors were dyed with H&E and Terminal-deoxynucleoitidyl Transferase Mediated Nick End Labeling (TUNEL), and distant tumors with proliferating cell nuclear antigen (PCNA). With another batch of mice, FCM was used to determine the mature dendritic cells (DCs) in bilateral tumor-draining lymph nodes on day 7. Immunofluorescence was conducted to investigate the infiltrating CD8-positive T cells in tumor tissues.

Statistical analysis

Data were described by mean and SD. Statistical analysis was undertaken with the use of GraphPad Prism. Student's t-test was applied to identify the differences between groups. The differences among groups were compared by one-way analysis of variance. A $p \leq 0.05$ indicated statistical significance.

RESULTS

Preparation and characterization of M@P-SOP nanomaterials

We first detected the physical properties of the NPs. TEM images (figure 2A,B) showed that both P-SOP and M@P-SOP exhibited a well-defined spherical shape with smooth surface, and a uniform outer layer about 20 nm thick was observed in M@P-SOP. Particle sizes and zeta-potentials of P-SOP and M@P-SOP were 213.80±1.47 and 233.37±2.20 nm, −10.73±0.71 and −19.43±0.12 mV, respectively (figure 2C,D). The increment of average diameter and decline of surface potential are probably ascribed to the coating of the negatively charged cell membrane with a thickness of around 10–20 nm.[38] The protein profiles of M@P-SOP were consistent with that of the extracted

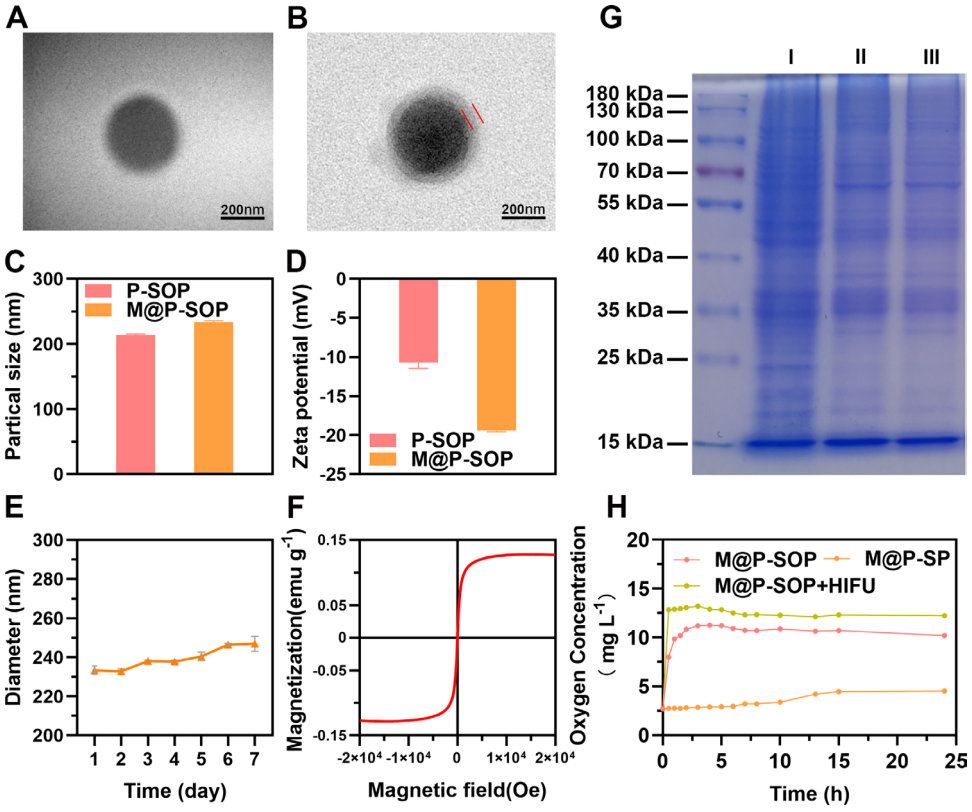

Figure 2 Characterization of M@P-SOP NPs. (A, B) Representative TEM images of P-SOP and M@P-SOP. Scale bars: 200 nm. (C) size distributions and (D) Zeta potentials of P-SOP and M@P-SOP. (E) Size changes of M@P-SOP over seven successive days in saline. (F) Magnetic hysteresis loops of M@P-SOP. (G) SDS-PAGE image of 4T1 tumor cells (I), 4T1 CCM (II) and M@P-SOP (III). (H) The O_2 release curves of P-SOP, M@P-SOP with or without HIFU exposure for 3 s at 120W. CCM, cancer cell membrane; HIFU, high-intensity focused ultrasound; SDS-PAGE, sodium dodecyl sulfate polyacrylamide gel electrophoresis; TEM, tumor microenvironment.

4T1 CCM, further validating the cell membrane translocation on M@P-SOP (figure 2G). After being suspended in saline, M@P-SOP appeared as a gray-brown solution without aggregation and obvious stratification (online supplemental figure S1A). The DiI-labeled M@P-SOP also exhibited homogenous size and high dispersity (online supplemental figure S1B). During 7 days preservation at 4°C, the size of NPs remained relatively stable over time (figure 2E). The high stability of M@P-SOP lays foundation for further in vivo biological applications.

The temperature-responsive property of M@P-SOP in online supplemental figure S1C confirmed the successful loading of PFH. Meanwhile, the O_2 concentration in solution was measured. The results showed that M@P-SOP showed an accelerated release rate of oxygen, reaching a peak at around 4 hours. While after HIFU irradiation, the O_2 release was close to 100% within 30 min (figure 2H), suggesting HIFU can trigger an instantaneous and burst O_2 release. The Fe EE was detected to be 70.08% and the paramagnetic property was further confirmed, validating SPIO was successfully loaded (figure 2F). To sum up, the above results indicate that a novel CCM-covering nanocarrier loaded with SPIO and O_2-carrying-PFH (M@P–SOP) is successfully synthesized.

Targeting efficiency of M@P-SOP

To investigate whether NPs coated with CCM had a higher ability of internalization, DiI-labeled P-SOP and M@P-SOP were separately co-incubated with 4T1 cells. By CLSM and FCM, we found that both of the two NPs exhibited time-dependent cell internalization behaviors, but the fluorescence intensity of M@P-SOP was stronger than that of P-SOP (online supplemental figure S2A,B), which indicated the tumor cells internalized more M@P-SOP NPs. Next, the homotypic targeting assay showed that 4T1 cells exhibited stronger M@P-SOP fluorescence than B16F10, MCF-7 and MDA-231 cells (online supplemental figure S2C,D), confirming that M@P-SOP preferred to accumulate in 4T1 rather than other tumor cells.

The tumor targeting behavior was also explored in vivo. DiR-labeled P-SOP and M@P-SOP were i.v. injected for living fluorescence imaging in homologous 4T1 tumor-bearing mice. The maximum fluorescence intensity of M@P-SOP was observed at the tumor site after 24 hours, which is much stronger than that of P-SOP ($p<0.01$) (online supplemental figure S2E,F). Given the excellent cancer accumulating ability of M@P-SOP, the therapeutic efficiency of subsequently performed HIFU may be markedly enhanced with minimal side effects.

US, PA and MR multimodal imaging in vitro and in vivo

The capacity of HIFU-stimulated USI was assessed in vitro and in vivo. online supplemental figure S3A–C shows that an enhanced acoustic signal was determined for PFH-encapsulated M@P-SP and M@P-SOP after HIFU in vitro, which was expected, as the thermal and cavitation effects of HIFU can cause PFH phase transition and MBs generation. The preliminary in vivo USI performance was assessed in a murine 4T1 tumor model. Results showed that the ultrasonic signals intensity were significantly increased in M@P-SOP with HIFU, while no obvious signal was detected in P-SOP without CCM coating (figure 3A,B, online supplemental figure S3F).

Owing to the superparamagnetic and photoacoustic properties of SPIO, the PAI/MRI capabilities of M@P–SOP were also assessed. As expected, online supplemental figure S3D,E shows that the PAI/T_2-weighted MRI signal intensity of M@P-SOP in vitro was noticeably dose-dependent and demonstrated a linear relationship. In addition, the dynamic PA/MR images in tumor of mice showed that the signals were evidently enhanced and peaked at 24 hours postinjection in M@P-SOP group, whereas that was much lower in non-targeted P-SOP group (figure 3C–F). These results demonstrated that M@P-SOP possessed tremendous potential for application as a contrast agent for US/PA/MR imaging to realize accurate diagnosis of tumor and image-guided therapies.

Evaluation of synergistic effect of M@P-SOP for HIFU therapy

To assess the synergistic efficacy of M@P-SOP for HIFU irradiation, fresh bovine liver was applied as the ex vivo model to visualize the ablated area of HIFU. As displayed in figure 4A, the ablated volume with M@P-SOP is significantly larger than control and PLGA without PFH cores (M@P and M@P-S), indicating the presence of PFH exerts a vital role in enhanced HIFU therapy. These results also provided a reference HIFU output (120 W, 3 s) for the subsequent experiments as it causes excellent therapeutic efficacy and may not destroy the adjacent tissue.

In vivo evaluations were further carried out to determine the ability of M@P-SOP in acting as a synergist for HIFU on 4T1 murine tumor model. As depicted in figure 4B,D, the acoustic signal at the tumor site is remarkably magnified after HIFU stimulation (120 W-3s) for M@P-SOP group, while the other groups (control, M@P, M@P-S) present no notable echo changes at the same HIFU dose. The tumor specimens were then taken out for TTC staining to indicate necrotic damages of tumor tissues. In accordance with the ex vivo results, the necrotic volume of tumor was much bigger and the EEF value was much lower in HIFU+M@P-SOP (figure 4C,E,F). Such a notable increase in tumor ablation volume indicated that the PFH-containing M@P-SOP can serve as a highly efficient SA for HIFU ablation.

In vivo antitumor performance and mechanism of M@P-SOP synergized with HIFU

Encouraged by the satisfactory results of M@P-SOP-enhanced HIFU ablation, we carefully evaluated the antitumor potency of M@P-SOP with HIFU using 4T1 breast cancer model. The mice were intravenously administrated with saline, M@P-SP or M@P-SOP with or without HIFU (120W, 3 s) applied to the tumor 24 hours postinjection (online supplemental figure S4A). As the representative photographs of tumors and average tumor weights showed, HIFU+M@P-SOP resulted in greatly delayed

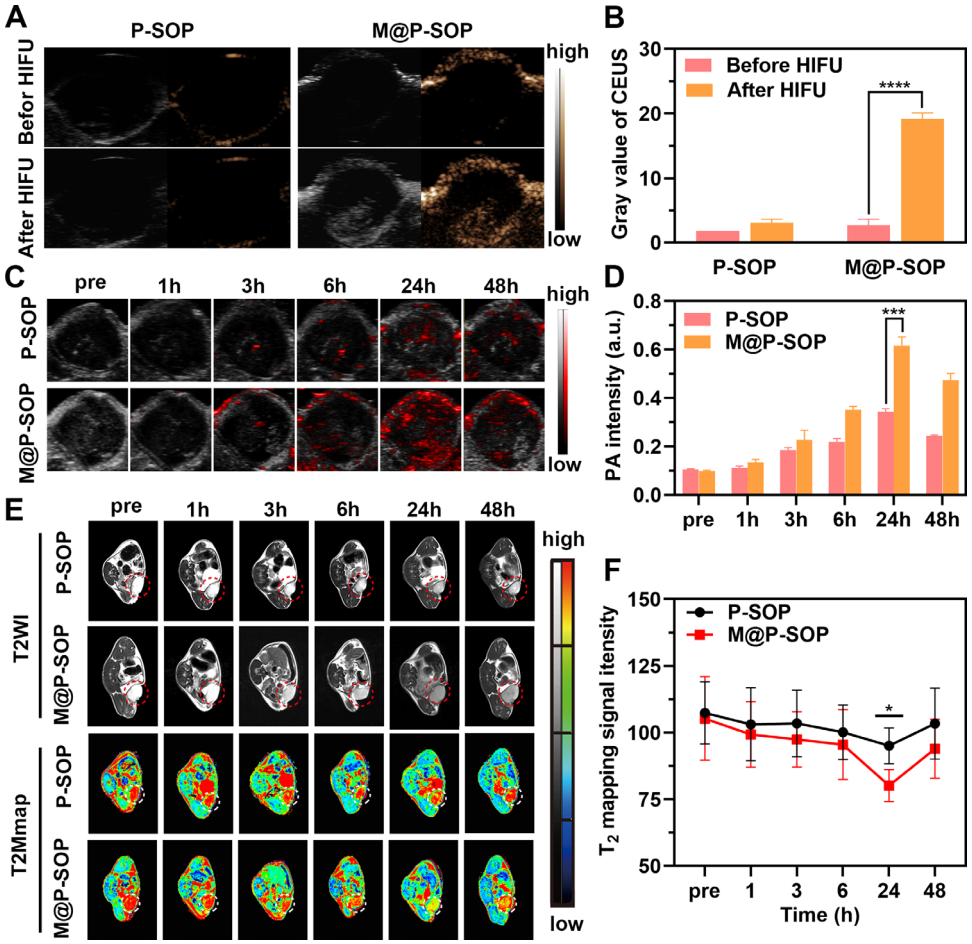

Figure 3 The multimodal imaging of nanoparticles in vitro and in vivo. (A) In vivo B-mode and contrast-enhanced ultrasound (CEUS) imaging of P-SOP or M@P-SOP before and after HIFU irradiation. (B) The quantitative analyses of a (n=3, t-test, ****p<0.0001). (C) In vivo PA images of P-SOP NPs and M@P-SOP NPs at pre, 1, 3, 6, 24, and 48 hours post intravenous injection. (D) The quantitative analyses of C (n=3, t-test, ***p<0.001). (E) In vivo T_2-weighted MRI of P-SOP and M@P-SOP at pre, 1, 3, 6, 24, and 48 hours post intravenous injection. (F) the quantitative analyses of E (n=3, t-test, *p<0.05). HIFU, high-intensity focused ultrasound.

tumor growth, while the other treatments exerted no or only slight impact on tumor growth (online supplemental figure S4B,C).

The potential underlying immune mechanism was next studied via immunofluorescence, FCM and ELISA. As displayed via confocal microscopic observation, mice treated with M@P-SOP+HIFU or M@P-SP+HIFU, especially the former, showed significantly increased the expression of calreticulin (CRT) (figure 5A), a representative damage associate molecular pattern revealing ICD of tumor cells.[39] By contrast, M@P-SP, M@P-SOP or HIFU treatment alone showed minimal influence on CRT in tumor tissue. Through analyzing the maturation degree of DCs inside tumor draining lymph nodes and spleens using FCM, we found HIFU+M@P-SOP exhibited the strongest ability to promote DC maturation (figure 5B,C,E,F). Correspondingly, HIFU+M@P-SOP could lead to greatly increased tumor-infiltrating T cells as compared with other groups by immunofluorescence (figure 5D), which suggested that the ICD and DC maturation mediated by HIFU+M@P-SOP triggered excellent antitumor immune responses.

However, the immunosuppressive TME, which is closely related to tumor hypoxia, can lead to invalid antitumor immunity. Enlightened by the effective oxygen load capacity of PFH, we subsequently assessed the efficacy of M@P-SOP in mitigating tumor hypoxia. In vitro hypoxic assay showed that the generation of O_2 displayed a positive correlation with the concentration of M@P-SOP under hypoxia conditions (figure 6A). Further in vivo immunofluorescence of tumor slices (figure 6B) revealed that the HIFU+M@P-SOP exhibited the markedly decreased tumor hypoxia signals (green) and HIF-1α level. These data demonstrated HIFU+M@P-SOP significantly increased O_2 content in tumor site and effectively improved the tumor hypoxia microenvironment.

Further, as an important component of the immunosuppressed TME, the percentage of protumor M2 macrophages decreased from 47.97% to 23.23%, while the frequencies of antitumor M1 macrophages increased from 32.39% to

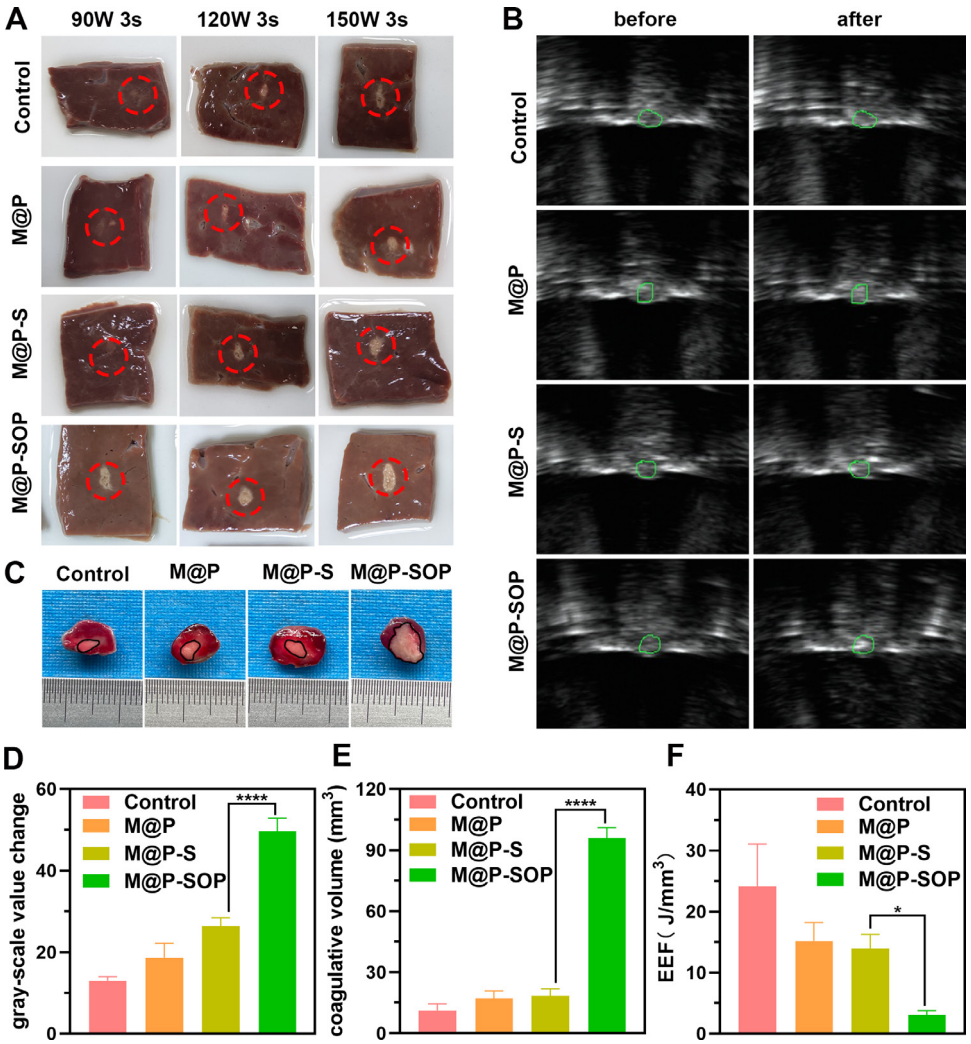

Figure 4 Evaluation of synergistic efficiency of HIFU therapy. (A) Digital photos of ablated bovine livers. (B) US images before and after HIFU stimulus. (C) The necrotic tumor volume evaluated by TTC staining. The tumor region was dyed red and coagulation necrosis region showed gray white. (D–F) Corresponding gray scale value, necrosis volume and EEF at targeted tumor site after HIFU irradiation (n=3, t-test, ****p<0.0001, *p<0.05). EEF, energy efficiency factor; HIFU, high-intensity focused ultrasound; TTC, 2,3,5-Triphenyltetrazolium chloride; US, ultrasound.

72.19% after HIFU+M@P-SOP (figure 6C,D). Correspondingly, it was uncovered that after HIFU+M@P-SOP, the content of IL-10, a protumorigenic cytokine secreted by M2-type macrophages, strikingly descending; in contrast, the content of IL-12, an antitumor cytokine secreted by M1-type macrophages, dramatically ascending. Moreover, the amount of TNF-α, an important antitumor signal, potently increased in HIFU+M@P-SOP (figure 6E–G).

In general, these results demonstrate that HIFU+M@P-SOP could notably increase the population of native M1-type macrophages and acquired cytotoxic T cells in tumor tissue. The high potency of this combinatorial strategy is probably attributed to M@P-SOP mediated tumor hypoxia mitigation and targeted HIFU enhancement.

Synergy and mechanism of HIFU with anti-PD-L1 on metastatic tumors

Inspired by the high potency of M@P-SOP-augmented HIFU in priming effective anti-tumor immunity, we thereby investigated the combination therapeutic efficacy of M@P-SOP+HIFU plus anti-PD-L1 immunotherapy against tumor metastasis. To this end, bilateral tumor-bearing mice were intravenously administrated with saline or M@P-SOP (5 mg/kg) with or without HIFU exposure (120 W, 3 s) 24 hours postinjection, then anti-PD-L1 antibody (1.5 mg/kg) was intravenously injected 1, 4 and 7 days post-HIFU (online supplemental figure S5A). By recording tumor size, we found that HIFU+NPs+anti-PD-L1 group could effectively prohibit both primary and distant tumor (mimic metastasis) growth (figure 7A,B and online supplemental figure S5B). By comparison, mice treated by HIFU+M@P-SOP, HIFU+anti-PD-L1, bare anti-PD-L1 or HIFU exhibited minimal inhibition effect on tumor growth. The body weights of mice kept stable during the observation period (figure 7C), indicating high biosafety of our strategy for biological application. Furthermore, H&E-stained images showed that HIFU+NPs+PD-L1 group exhibited fewer cells with nuclear dying

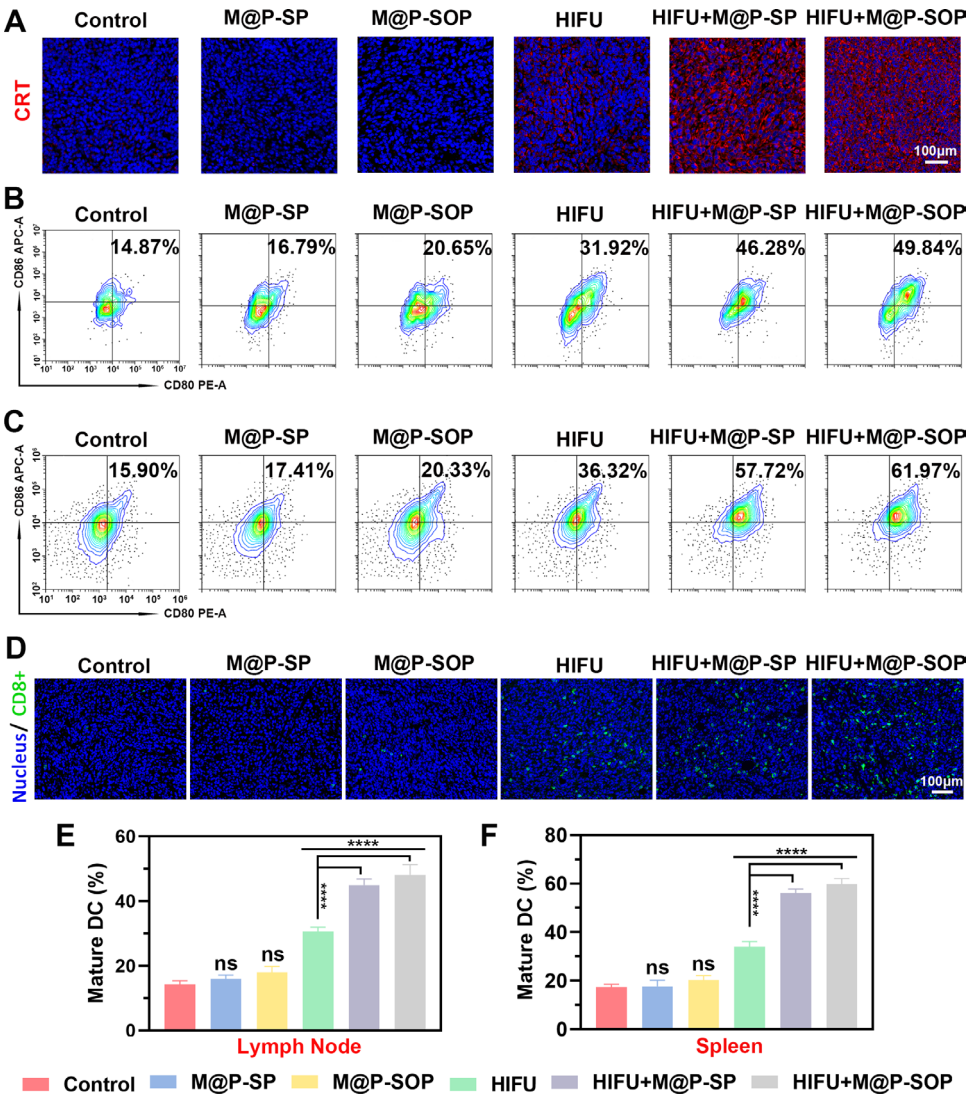

Figure 5 In vivo therapeutic mechanism of M@P-SOP with HIFU. (A) Immunofluorescence staining of CRT in tumor slices after various treatments. (B, C) FCM analysis of DCs maturation in lymph nodes (B) and spleen (C) initiated by various treatments in vivo. (D) Immunofluorescence images of tumor slices displaying population of CD8-positive cells for various groups of mice. (E, F) Statistical data of (B, C) respectively (n=3, one-way ANOVA, ****p<0.0001). ANOVA, analysis of variance; DC, dendritic cell; FCM, flow cytometry; CRT, calreticulin; HIFU, high-intensity focused ultrasound; ns, not significant.

blue, indicating the heaviest cell necrosis in primary tumor by contrast with other groups, which was in line with TUNEL results. The PCNA staining of distant tumor proved that HIFU+NPs+PD-L1 caused the strongest proliferation inhibition (figure 7D). Taken together, this combined ablation with anti-PD-L1 regimen resulted in robust synergistic anticancer effect against primary and remote tumor with negligible side effects.

By detailed immune analysis, as demonstrated in figure 7E–I, the number of mature DCs in the primary and distant tumor-draining lymph nodes were significantly larger in HIFU+NPs+PD-L1 group than in other groups by FCM. Also, immunofluorescence demonstrated significantly augmented $CD8^+$ T cell infiltration among both ablated and contralateral, non-ablated tumors after NPs-enhanced HIFU plus anti-PD-L1 therapy. These results demonstrated that combining M@P-SOP enhanced-HIFU with anti-PD-L1 could elicit potent antitumor immunity to prevent tumor metastasis.

From a clinical perspective, the biosecurity of NPs is the major concern of investigators before biological applications. As shown in online supplemental figure S6A, both P-SOP and M@P-SOP showed negligible disturbance on cellular viability even at 10 mg/mL. Further in vivo toxicity study showed that no noticeable difference of the blood routine and serum biochemical parameters were observed between control and M@P-SOP-treated group (online supplemental figure S6B). Furthermore, no significant pathological abnormality was discovered in H&E images of vital organs over time (online supplemental figure S6C), validating the good biosafety of the NPs in our system.

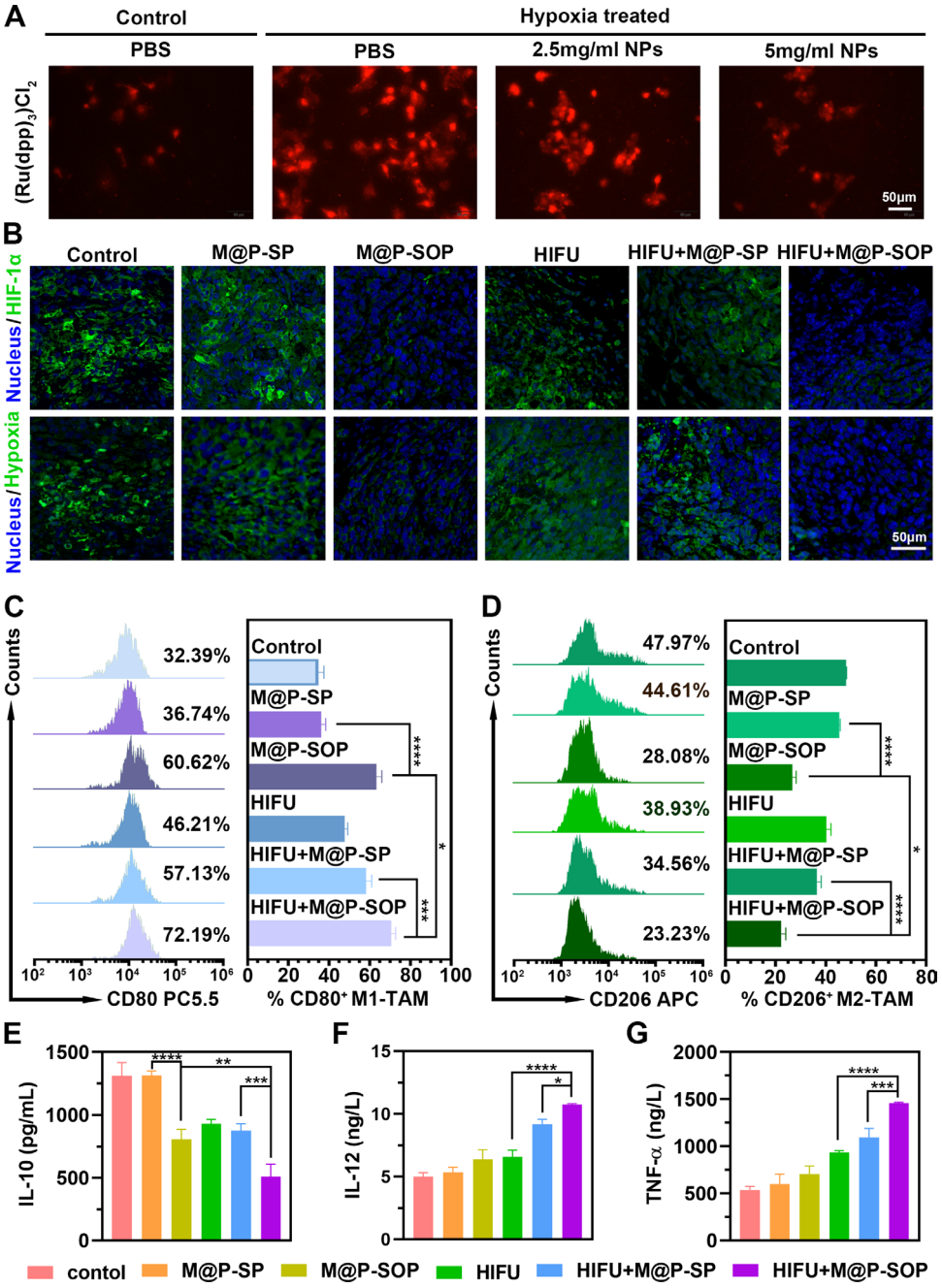

Figure 6 Related mechanism of M@P-SOP with HIFU in vivo. (A) CLSM images of 4T1 cells exposed to PBS under normoxia condition or M@P-SOP (0, 2.5, 5 mg/mL) in an anoxic environment for 24 hours. Scale bar is 50 μm. (B) Immunofluorescence images of tumor slices incubated with anti-pimonidazole or HIF-1α antibody. Scale bar is 50 μm. (C, D) FCM data displaying tumor infiltrating $CD80^+CD11b^+F4/80^+$ cells (C) and $CD206^+CD11b^+F4/80^+$ cells (D) in tumors of mice treated differently (n=3, one-way ANOVA, *p<0.05, ***p<0.001, ****p<0.0001). (E–G) Cytokine (IL-10, IL-12 and TNF-α) concentrations in serum sample from various groups of mice by ELISA assay (n=3, one-way ANOVA, *p<0.05, **p<0.01, ***p<0.001, ****p<0.0001). ANOVA, analysis of variance; FCM, flow cytometry; HIFU, high-intensity focused ultrasound.

DISCUSSION

The clinical outcome of immunotherapy is unsatisfied in patients with immunologically 'cold' tumor, commonly manifested by low levels of neoantigens, lack of tumor-infiltrating cytotoxic T cells and presence of immunosuppressive TME.[40–44] HIFU offers a readily way to resist many of these detrimental aspects. Multiple preclinical studies have demonstrated combining HIFU with ICIs has improves the survival and response rates of immunotherapies.[17 45] By stimulating ICD, HIFU can trigger an in situ vaccine effect, eliciting a protective antitumor immune response.[46 47] However, the immunity activated by HIFU is weak or incomplete because it is insufficient to overcome immunosuppressive TME.[2] To accentuate the antitumor capacity of HIFU, we developed a multifunctional NP (M@P-SOP) for the specific purpose of regulating the acoustic and immune TME.

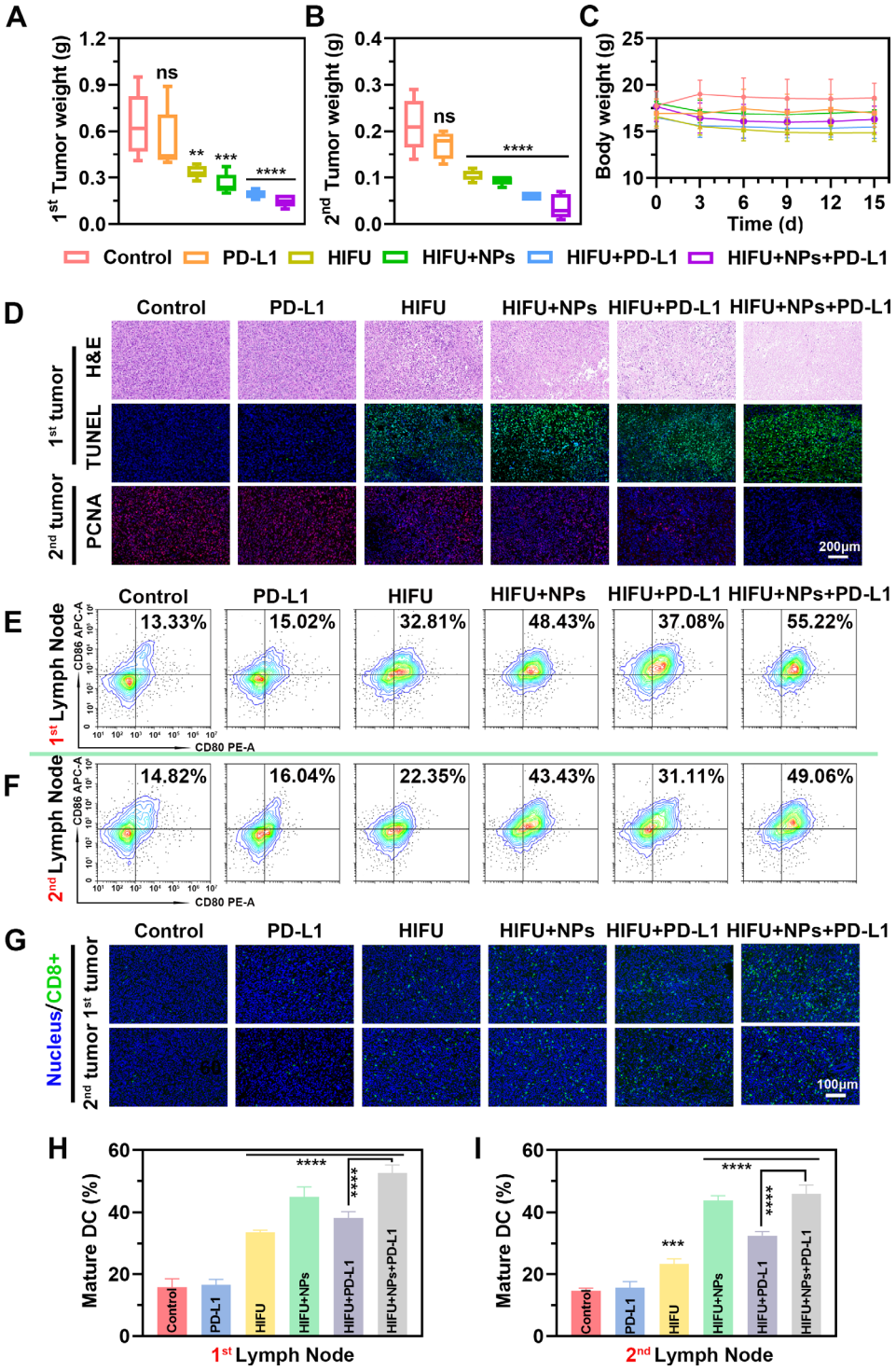

Figure 7 The therapeutic efficacy of M@P-SOP facilitated HIFU with PD-L1 blockade on tumor metastases in vivo. (A, B) Weights of primary (A) and mimic distant (B) tumors with various treatments (n=5, one-way ANOVA, **p<0.01, ***p<0.001, ****p<0.0001). (C) Body weight change of mice during observation period. (D) H&E, TUNEL and PCNA images of cancer tissues after various treatments. TUNEL and PCNA positive area showed green and red respectively. Blue signals displayed the cell nuclei dyed with DAPI. Scale bar: 200 μm. (E, F) FCM analysis of DCs maturation in the tumor draining lymph nodes of primary (E) and remote (F) tumors initiated by different treatments. (G) Immunofluorescence images of CD8-positive (green) cells in tumor tissues. Scale bar: 100 μm. (H, I) Statistical data of E and F, respectively (n=3, one-way ANOVA, **p<0.01, ***p<0.001, ****p<0.0001). ANOVA, analysis of variance; DCs, dendritic cells; FCM, flow cytometry; HIFU, high-intensity focused ultrasound; PCNA, proliferating cell nuclear antigen.

After systemic administration, the as-prepared M@P–SOP acquired high tumor accumulation due to the homologous targeting capacity of CCM coating. On HIFU exposure at the tumor site, the transformed PFH MBs robustly improved the AET and enhanced the efficacy of HIFU irradiation. Simultaneously, the ICD of tumor cells was induced and O_2 releasing from M@P-SOP attenuated tumor hypoxia, thus alleviating the immunosuppressive TME. As a result, M@P-SOP augmented-HIFU therapy could effectively elicit potent anticancer immunity, particularly with anti-PD-L1 which further activates the CTLs, consequently suppress primary and mimic distant tumor growth.

Currently, with a glimpse at the recent progress of HIFU, the combined regimes of HIFU and immunotherapy (eg, CTLA-4[17] or PD-1/PD-L1)[48] could maximize benefits of this ablative therapy. Compared with reported combinatorial modalities, our developed strategy of NP-enhanced HIFU with PD-L1 blockade offers obvious superiority. First, the elaborately designed multifunctional biomimetic M@P-SOP nanocapsules in this work could efficiently facilitate HIFU ablation with reduced total US energy required (120W, 3s), which is even lower than the parameter settings (150W, 5s) of a previous report using the same HIFU machine.[10] The main mechanism of the synergy for M@P-SOP in HIFU ablation may be the following: the accumulation of the NPs in tumor tissues was potentiated owing to their nano-sizes and the targeted CCM covering, which results in sufficient MBs generated to exert the synergistic effect; the presence of O_2 carrying PFH could serve as a liquid-to-gas phase-transformable agent and release O_2 bubbles under HIFU irradiation, which dramatically alter AET of the tumor, consequently augment US energy deposition in the focal region. Moreover, the O_2 carried by PFH in M@P-SOP can favorably modulate the immunosuppressive hypoxic TME, repolarizing TAMs to the immunostimulatory M1 subtype. Typically, M1-type macrophages secrete proinflammatory cytokines (TNF-α, IL12, etc) and trigger an antitumor immune response. While the alternative M2-type macrophages exert inhibitory roles by producing immunosuppressive cytokines such as IL-10.[49] As hypoxic TAMs (more resemble an M2-like phenotype) release factors that diminish T cell activation and proliferation,[50] phenotypic control of macrophages by tumor hypoxia relief via oxygen-carrying NPs may potentially serve as an adjunctive therapeutic modality for cancer immunotherapy. Accordingly, the ICD by HIFU, immunosuppressive microenvironment attenuation by O_2 releasing from NPs and T-cell response enhancement by anti-PD-L1 could collectively activate systemic immune response, consequently suppress both primary and untreated remote tumor growth, as demonstrated in 4T1 tumor xenograft in mice. Finally, the M@P-SOP could also realize complementary multimodal-imaging including USI by PFH, T_2-weighted MRI and PAI by SPIO. US/MR/PA multimodality imaging is an integrated approach for cancer imaging and NPs biological distribution monitoring, which can complement the strengths of individual imaging, with real-time observation of USI,[12] anatomical resolution of MRI, and high spatial resolution of PAI.[23] Thus, by introduction of M@P-SOP, we provide a precision platform for HIFU facilitation.

In summary, we proposed a rational combination of M@P-SOP-augmented HIFU and anti-PD-L1 blockade for high-efficient cancer treatment. In view of HIFU-based cancer treatment has already been applied in clinic, this may be a promising therapeutic modality for clinical translation. The possible benefit is not limited in application to breast cancer, but has potential for any type of solid tumor. Moreover, combinatorial modalities of such immunogenic ablation treatment and various immunotherapy beyond anti-PD-L1 also deserve further explorations owing to its simplicity, generality and practicability for cancer treatment.

Author affiliations
[1]Department of Ultrasound, The Second Affiliated Hospital of Chongqing Medical University, Chongqing, China
[2]Institute of Ultrasound Imaging of Chongqing Medical University, Chongqing, China
[3]Department of Ultrasound, Chongqing General Hospital, Chongqing, China
[4]State Key Laboratory of Ultrasound in Medicine and Engineering, College of Biomedical Engineering, Chongqing Medical University, Chongqing, China
[5]Department of ultrasound, The Third People's Hospital of Chengdu City, Chengdu, People's Republic of China

Acknowledgements We appreciate Profs. Zhigang Wang, Jianli Ren, and Haitao Ran for their helpful suggestions.

Contributors RT: Manuscript editing and experimental studies; HH and XL: Research design and experimental studies; YC, LW and QC: Manuscript smoothing; NW, YH, XG, CC and YZ: Statistical analysis; XX and MZ: Literature research; QW, FL and YZ: supervised the research; PL: Study concepts. PL is the guarantor.

Funding This work was funded by the Yong and Middle-age High-level Medical Personnel Training Project Foundation of Chongqing (2019GDRC006), National Natural Science Foundation of China (8197071491, 81971636, 82272025), the key project of Chongqing Natural Science Foundation (cstc2021jcyj-msxmX0220), Chongqing talents: Innovation and entrepreneurship leading talents (CQYC2020030355).

Competing interests None declared.

Patient consent for publication Not applicable.

Provenance and peer review Not commissioned; externally peer reviewed.

Data availability statement All data relevant to the study are included in the article or uploaded as online supplemental information.

ORCID iD
Pan Li http://orcid.org/0000-0002-0316-0355

REFERENCES

1 Mai X, Chang Y, You Y, *et al*. Designing intelligent nano-bomb with on-demand site-specific drug burst release to synergize with high-intensity focused ultrasound cancer ablation. *J Control Release* 2021;331:270–81.
2 Fite BZ, Wang J, Kare AJ, *et al*. Immune modulation resulting from MR-guided high intensity focused ultrasound in a model of murine breast cancer. *Sci Rep* 2021;11:927.
3 Zhong X, Zhang M, Tian Z, *et al*. The Study of Enhanced High-Intensity Focused Ultrasound Therapy by Sonodynamic N_2O Microbubbles. *Nanoscale Res Lett* 2019;14:381.
4 Xu D, Zou W, Luo Y, *et al*. Feasibility between bifidobacteria targeting and changes in the acoustic environment of tumor tissue for synergistic HIFU. *Sci Rep* 2020;10:7772.
5 Tang Y, Chen C, Jiang B, *et al*. *Bifidobacterium bifidum*-Mediated Specific Delivery of Nanoparticles for Tumor Therapy. *Int J Nanomedicine* 2021;16:4643–59.
6 Zhang N, Cai X, Gao W, *et al*. A multifunctional theranostic Nanoagent for dual-mode image-guided HIFU/Chemo- synergistic cancer therapy. *Theranostics* 2016;6:404–17.
7 Wang Y, Chen C, Luo Y, *et al*. Experimental study of tumor therapy mediated by multimodal imaging based on a biological targeting synergistic agent. *Int J Nanomedicine* 2020;15:1871–88.
8 Chen Y, Chen H, Shi J. Nanobiotechnology promotes noninvasive high-intensity focused ultrasound cancer surgery. *Adv Healthc Mater* 2015;4:158–65.
9 Sun H, Liu K, Huang J, *et al*. FAM111B, a direct target of p53, promotes the malignant process of lung adenocarcinoma. *Onco Targets Ther* 2019;12:2829–42.
10 Zhang Y, Yong L, Luo Y, *et al*. Enhancement of HIFU ablation by sonosensitizer-loading liquid fluorocarbon nanoparticles with pre-targeting in a mouse model. *Sci Rep* 2019;9:6982.
11 Zeng Z, Liu J-B, Peng C-Z. Phase-changeable nanoparticle-mediated energy conversion promotes highly efficient high-intensity focused ultrasound ablation. *Curr Med Chem* 2022;29:1369–78.
12 Tang H, Guo Y, Peng L, *et al*. In vivo targeted, responsive, and synergistic cancer Nanotheranostics by magnetic resonance imaging-guided synergistic high-intensity focused ultrasound ablation and chemotherapy. *ACS Appl Mater Interfaces* 2018;10:15428–41.
13 You Y, Wang Z, Ran H, *et al*. Nanoparticle-enhanced synergistic HIFU ablation and transarterial chemoembolization for efficient cancer therapy. *Nanoscale* 2016;8:4324–39.
14 Zhou Y, Wang Z, Chen Y, *et al*. Microbubbles from gas-generating perfluorohexane nanoemulsions for targeted temperature-sensitive ultrasonography and synergistic HIFU ablation of tumors. *Adv Mater* 2013;25:4123–30.
15 Li Q, Zhang J, Li J, *et al*. Glutathione-Activated NO-/ROS-Generation nanoparticles to modulate the tumor hypoxic microenvironment for enhancing the effect of HIFU-Combined chemotherapy. *ACS Appl Mater Interfaces* 2021;13:26808–23.
16 Tolba MF, Elghazaly H, Bousoik E, *et al*. Novel combinatorial strategies for boosting the efficacy of immune checkpoint inhibitors in advanced breast cancers. *Clin Transl Oncol* 2021;23:1979–94.
17 Eranki A, Srinivasan P, Ries M, *et al*. High-Intensity focused ultrasound (HIFU) triggers immune sensitization of refractory murine neuroblastoma to checkpoint inhibitor therapy. *Clin Cancer Res* 2020;26:1152–61.
18 Liu Q, Zhang W, Jiao R, *et al*. Rational nanomedicine design enhances clinically physical Treatment-Inspired or combined immunotherapy. *Adv Sci* 2022;9:2203921.
19 Lei L, Cai S, Zhang Y, *et al*. Structure Inversion-Bridged sequential amino acid metabolism disturbance potentiates Photodynamic-Evoked immunotherapy. *Adv Funct Mater* 2022;32:2103394.
20 Chavez M, Silvestrini MT, Ingham ES, *et al*. Distinct immune signatures in directly treated and distant tumors result from TLR adjuvants and focal ablation. *Theranostics* 2018;8:3611–28.
21 Silvestrini MT, Ingham ES, Mahakian LM, *et al*. Priming is key to effective incorporation of image-guided thermal ablation into immunotherapy protocols. *JCI Insight* 2017;2:e90521.
22 Chen W-S, Shen C-C, Wang J-C, *et al*. Single-element ultrasound transducer for combined vessel localization and ablation. *IEEE Trans Ultrason Ferroelectr Freq Control* 2011;58:766–75.
23 Zhou T, Liang X, Wang P, *et al*. A hepatocellular carcinoma targeting Nanostrategy with Hypoxia-Ameliorating and photothermal abilities that, combined with immunotherapy, inhibits metastasis and recurrence. *ACS Nano* 2020;14:12679–96.
24 Multhoff G, Vaupel P. Hypoxia compromises anti-cancer immune responses. *Adv Exp Med Biol* 2020;1232:131–43.
25 Sebestyén A, Kopper L, Dankó T, *et al*. Hypoxia signaling in cancer: from basics to clinical practice. *Pathol Oncol Res* 2021;27:1609802.
26 Ma X, Yao M, Shi J, *et al*. High intensity focused Ultrasound-Responsive and ultrastable Cerasomal perfluorocarbon Nanodroplets for alleviating tumor multidrug resistance and epithelial-mesenchymal transition. *ACS Nano* 2020;14:15904–18.
27 Zhu J, Li Z, Zhang C, *et al*. Single enzyme loaded nanoparticles for combinational ultrasound-guided focused ultrasound ablation and hypoxia-relieved chemotherapy. *Theranostics* 2019;9:8048–60.
28 Liu T, Zhang N, Wang Z, *et al*. Endogenous Catalytic Generation of O_2 Bubbles for In Situ Ultrasound-Guided High Intensity Focused Ultrasound Ablation. *ACS Nano* 2017;11:9093–102.
29 Zhang C, Yan Q, Li J, *et al*. Nanoenabled tumor oxygenation strategies for overcoming Hypoxia-Associated immunosuppression. *ACS Appl Bio Mater* 2021;4:277–94.
30 Xu C-H, Ye P-J, Zhou Y-C, *et al*. Cell membrane-camouflaged nanoparticles as drug carriers for cancer therapy. *Acta Biomater* 2020;105:1–14.
31 Tian X, Shi A, Wu J. Construction of biomimetic-responsive nanocarriers and their applications in tumor targeting. *Anticancer Agents Med Chem* 2022;22:2255-2273.
32 Xiong J, Wu M, Chen J, *et al*. Cancer-Erythrocyte hybrid Membrane-Camouflaged magnetic nanoparticles with enhanced Photothermal-Immunotherapy for ovarian cancer. *ACS Nano* 2021;15:19756–70.
33 Chen Z, Zhao P, Luo Z, *et al*. Cancer cell Membrane-Biomimetic nanoparticles for Homologous-Targeting Dual-Modal imaging and photothermal therapy. *ACS Nano* 2016;10:10049–57.
34 Liu Z, Wan P, Yang M, *et al*. Cell membrane camouflaged cerium oxide nanocubes for targeting enhanced tumor-selective therapy. *J Mater Chem B* 2021;9:9524–32.
35 Luo Y, Xu D, Gao X, *et al*. Nanoparticles conjugated with bacteria targeting tumors for precision imaging and therapy. *Biochem Biophys Res Commun* 2019;514:1147–53.
36 Liu L, Wang Y, Guo X, *et al*. A biomimetic polymer magnetic nanocarrier polarizing tumor-associated macrophages for potentiating immunotherapy. *Small* 2020;16:2003543.
37 Wei Y, Wang Z, Yang J, *et al*. Reactive oxygen species / photothermal therapy dual-triggered biomimetic gold nanocages nanoplatform for combination cancer therapy via ferroptosis and tumor-associated macrophage repolarization mechanism. *J Colloid Interface Sci* 2022;606:1950–65.
38 Li Z, Yang G, Han L, *et al*. Sorafenib and triptolide loaded cancer cell-platelet hybrid membrane-camouflaged liquid crystalline lipid nanoparticles for the treatment of hepatocellular carcinoma. *J Nanobiotechnology* 2021;19:360.
39 Yang Z, Tao D, Zhong W, *et al*. Perfluorocarbon loaded fluorinated covalent organic polymers with effective sonosensitization and tumor hypoxia relief enable synergistic sonodynamic-immunotherapy. *Biomaterials* 2022;280:121250.
40 Zhang Y, Sriramaneni RN, Clark PA, *et al*. Multifunctional nanoparticle potentiates the in situ vaccination effect of radiation therapy and enhances response to immune checkpoint blockade. *Nat Commun* 2022;13:4948.
41 Duan Q, Zhang H, Zheng J, *et al*. Turning cold into hot: firing up the tumor microenvironment. *Trends Cancer* 2020;6:605–18.
42 Bonaventura P, Shekarian T, Alcazer V, *et al*. Cold tumors: a therapeutic challenge for immunotherapy. *Front Immunol* 2019;10:168.
43 Wu H, Li H, Liu Y, *et al*. Blockading a new NSCLC immunosuppressive target by pluripotent autologous tumor vaccines magnifies sequential immunotherapy. *Bioact Mater* 2022;13:223–38.
44 Wang D, Zhang M, Zhang Y, *et al*. Intraparticle Double-Scattering-Decoded Sonogenetics for augmenting immune checkpoint blockade and CAR-T therapy. *Adv Sci* 2022;9:2203106.
45 Mouratidis PXE, Costa M, Rivens I, *et al*. Pulsed focused ultrasound can improve the anti-cancer effects of immune checkpoint inhibitors in murine pancreatic cancer. *J R Soc Interface* 2021;18:20210266.
46 Cirincione R, Di Maggio FM, Forte GI, *et al*. High-Intensity focused Ultrasound- and radiation therapy-induced Immuno-Modulation: comparison and potential opportunities. *Ultrasound Med Biol* 2017;43:398–411.
47 Zhang Y, Deng J, Feng J, *et al*. Enhancement of antitumor vaccine in ablated hepatocellular carcinoma by high-intensity focused ultrasound. *World J Gastroenterol* 2010;16:3584–91.
48 Abe S, Nagata H, Crosby EJ, *et al*. Combination of ultrasound-based mechanical disruption of tumor with immune checkpoint blockade modifies tumor microenvironment and augments systemic antitumor immunity. *J Immunother Cancer* 2022;10:e003717.
49 Chen Y, Song Y, Du W, *et al*. Tumor-associated macrophages: an accomplice in solid tumor progression. *J Biomed Sci* 2019;26:78.
50 Henze A-T, Mazzone M. The impact of hypoxia on tumor-associated macrophages. *J Clin Invest* 2016;126:3672–9.